

Studying the relationship between X-ray emission and accretion in AGNs using the XMM-Newton Bright Serendipitous Survey

R. Fanali,^{1,2} A. Caccianiga,¹ P. Severgnini,¹ R. Della Ceca,¹ E. Marchese,²
 F.J. Carrera,³ A. Corral,⁴ S. Mateos³

¹*INAF-Osservatorio Astronomico di Brera, via Brera 28, I-20121 Milan, Italy*

²*Università degli Studi di Milano Bicocca, Piazza Della Scienza 3, 20126 Milano, Italy*

³*Instituto de Fisica de Cantabria (CSIC-UC), Avenida de los Castros, 39005 Santander, Spain*

⁴*National Observatory of Athens (NOA), Palaia Penteli, 15236, Athens, Greece*

October 4, 2018

ABSTRACT

We study the link between the X-ray emission in radio-quiet AGNs and the accretion rate on the central Supermassive Black Hole using a statistically well-defined and representative sample of 71 type 1 AGNs extracted from the XMM-Newton Bright Serendipitous Survey. We search and quantify the statistical correlations between some fundamental parameters that characterize the X-ray emission, i.e. the X-ray spectral slope, Γ , and the X-ray “loudness”, and the accretion rate, both absolute (\dot{M}) and normalized to the Eddington luminosity (Eddington ratio, λ). We parametrize the X-ray loudness using three different quantities: the bolometric correction, K_{bol} , the two-point spectral index α_{OX} and the disk/corona luminosity ratio. We find that the X-ray spectral index depends on the normalized accretion rate while the “X-ray loudness” depends on both the normalized and the absolute accretion rate. The dependence on the Eddington ratio, in particular, is probably induced by the $\Gamma - \lambda$ correlation. The two proxies usually adopted in the literature to quantify the X-ray loudness of an AGN, i.e. K_{bol} and α_{OX} , behave differently, with K_{bol} being more sensitive to the Eddington ratio and α_{OX} having a stronger dependence with the absolute accretion. The explanation of this result is likely related to the different sensitivity of the two parameters to the X-ray spectral index.

Key words: galaxies: active - galaxies: nuclei - quasars: general - X-rays: galaxies

1 INTRODUCTION

The engine of Active Galactic Nuclei (AGNs) is powered by the accretion of matter onto the Supermassive Black Hole (SMBH), placed in the center of the host galaxy: the matter is heated (10^5 - 10^6 K) through viscous and magnetic processes and forms an accretion disk around the SMBH emitting in the UV-optical region. A fraction of energy is also emitted in the X-ray band with a spectrum that can be represented, at first order, by a power-law from 0.1 to 100 keV at rest-frame. In the now accepted disk-corona model (Haardt & Maraschi 1991), the X-rays are produced in a hot ($T=10^8$ - 10^9 K) corona, reprocessing the primary UV-optical emission of the disk via inverse-Compton mechanism. X-rays are a probe of accretion since they are produced in the very inner part of the nucleus and carry direct information on the physics very close to the SMBH. For instance, the hard X-ray

spectral index (Γ) gives direct information about the energy distribution of the electrons in the corona, while the intensity of the X-ray emission with respect to the UV-optical emission quantifies the relative importance between disk and corona. This latter quantity is often parametrized with the X-ray bolometric correction K_{bol} (e.g. Vasudevan & Fabian 2009), defined as the ratio between bolometric luminosity and 2 – 10 keV luminosity, or with the two-point-spectral index α_{OX} (e.g. Vignali et al. 2003), defined between 2500Å and 2 keV. The different values of X-ray spectral index and of the disk/corona luminosity ratio observed from source to source are likely a consequence of fundamental differences in the physical parameters of the central engine.

First studies, essentially based on *ROSAT* data, suggested correlations between the “soft” spectral index $\Gamma_{(0.5-2.4)\text{keV}}$ and the Full Width at Half Maximum (FWHM) of $H\beta$ emission line coming from the Broad

Line Region (BLR, Wang, Brinkmann & Bergeron 1996, Laor et al. 1997, Sulentic, Marziani & Dultzin-Hacyan 2000, Grupe et al. 2004). Assuming that BLR dynamics is directly dependent on the black hole mass, this correlation was suggesting a direct link between $\Gamma_{(0.5-2.4)\text{keV}}$ and some physical parameters like the black hole mass or accretion rate. In particular, it was suggested that the main physical driver of this correlation is the accretion rate normalized to the Eddington luminosity¹ (Eddington ratio): sources accreting close to the Eddington limit produce the steepest values of $\Gamma_{(0.5-2.4)\text{keV}}$ (Wang, Watarai & Mineshige 2004, Laor et al. 1997, Sulentic et al. 2000, Grupe et al. 2004). However, since the measured value of $\Gamma_{0.5-2.4\text{keV}}$ can be significantly contaminated by the presence of a spectral component called “soft excess”², it was difficult to establish on a firm ground whether it was the slope of the primary emission that correlates with the accretion rate or, instead, it was the intensity of the soft excess.

Using *ASCA* observations, Brandt et al. (1997) and Wang, Watarai & Mineshige (2004) have found that also the “hard” spectral slope ($\Gamma_{(2-10)\text{keV}}$) has a strong dependence with the $FWHM(H\beta)$. Since the 2-10 keV energy range is not affected by the “soft excess”, this result was considered as a compelling indication that the slope of the primary component of the X-ray emission actually correlates with $FWHM(H\beta)$. First studies made with *XMM-Newton*, *Chandra* and *Swift-XRT* have further suggested the possible presence of a second trend, i. e. an anti-correlation between $\Gamma_{(2-10)\text{keV}}$ and the black hole mass M_{BH} (Porquet et al. 2004, Piconcelli et al. 2005). The availability of hard X-ray data from *XMM-Newton* and *Chandra* and of statistical relations that allow the systematic computation of M_{BH} on large numbers of AGNs have produced in the very recent years a big leap forward on this kind of study, extending the analysis on significantly larger samples, including up to a few hundreds of sources (Kelly et al. 2008, Gu & Cao 2009, Shemmer et al. 2008, Risaliti, Young & Elvis 2009, Zhou & Zhang 2010, Grupe et al. 2010). These studies seem to confirm the presence of a correlation between the hard Γ and the Eddington ratio (Grupe et al. 2010, Risaliti et al. 2009) with some exceptions (Bianchi et al. 2009). Shemmer et al. (2008) have also demonstrated that the observed strong anti-correlation usually observed between Γ and $FWHM(H\beta)$ is a secondary correlation induced by the dependence between Γ and the Eddington ratio.

Also the bolometric correction is expected to be related to the physical parameters that regulate the accretion mechanism. A possible dependence of the K_{bol} with the luminosity has been suggested (Marconi et al. 2004, Hopkins et al. 2007), but more recent observations seem to point out that the principal dependence is between K_{bol} and the Eddington ratio (Vasudevan & Fabian 2007, Kelly et al. 2008, Vasudevan & Fabian 2009, Lusso et al. 2012). An alternative way to study the relative intensity between disk and corona is through the α_{OX} , de-

fining as the slope between 2500Å and 2 keV. Past studies generally found a strong correlation between α_{OX} and L_{UV} (e.g. Vignali et al. 2003, Marchese et al. 2012) or L_{bol} (Kelly et al. 2008, Shemmer et al. 2008) while a dependence of α_{OX} with the Eddington ratio is usually weak or absent (Young, Elvis & Risaliti 2010), contrary to what has been found for K_{bol} . This is quite surprising since K_{bol} and α_{OX} are both supposed to be proxies of the disk/corona relative intensity and therefore, they are somehow expected to behave in a similar way.

In this paper we investigate the link between X-ray properties and the accretion rate by analyzing a well defined sample of type 1 AGNs selected from the XMM-Newton Bright Serendipitous survey (XBS). In particular, we study the spectral index Γ estimated in the energy range 0.5 – 10 keV and 2 – 10 keV and three different parameters that quantify the “X-ray loudness” i.e. the bolometric correction K_{bol} , the α_{OX} and the disk/corona luminosity ratio (that is the ratio between the accretion disk luminosity and the 0.1 – 100 keV X-ray luminosity). The approach followed in this study is to search for statistically significant correlations between these parameters and the value of accretion rate, both absolute and normalized to Eddington luminosity.

The structure of the paper is the following: in Section 2 we describe the survey, the sample selection and the parameters used for our work; in Section 3 we describe the statistical analysis used to find the correlations between the parameters, taking into account a number of potential biases. In Section 4 we present our results. Finally, in Section 5 we report the summary and conclusions.

We assume here a flat Λ CDM cosmology with $H_0 = 65$ km s⁻¹ Mpc⁻¹, $\Omega_{\Lambda} = 0.7$ and $\Omega_M = 0.3$.

2 XMM-NEWTON BRIGHT SERENDIPITOUS SURVEY

The XMM-Newton Bright Serendipitous survey (XBS survey) is a wide-angle (~ 28 sq. deg) high Galactic latitude ($|b| > 20^\circ$) survey based on the XMM-Newton archival data. It is composed of two flux-limited samples: the XMM Bright Source Sample (BSS, 0.5-4.5 keV band, 389 sources) and the XMM Hard Bright Source Sample (HBSS, 4.5-7.5 keV band, 67 sources, with 56 sources in common with the BSS sample), having a flux limit of $\sim 7 \times 10^{-14}$ erg cm⁻² s⁻¹ in both energy selection bands. Selection criteria and properties of these samples are described in Della Ceca et al. (2004). The XBS is composed of sources that are detected serendipitously in the field-of-view of the XMM-Newton pointing, thus excluding the targets of the observations. For this reason the XBS can be considered as representative of the X-ray sky down to its flux limit.

To date, the spectroscopic identification level has reached 98% and 100% in the BSS and the HBSS samples, respectively. Most of the spectroscopic identifications are presented and discussed in Caccianiga et al. (2007, 2008).

The availability of good XMM-Newton data for the sources in the XBS sample, spanning the energy range between ~ 0.3 and ~ 10 keV, allowed us to perform a reliable X-ray spectral analysis for almost every AGNs of the sample (Corral et al. 2011).

¹ The Eddington luminosity is a theoretical limit beyond which the accretion process stops for effect of radiation pressure

² The “soft excess” is an excess of counts, at energies below 2 keV, with respect to the power-law component fitted at higher energies (typically between 2 and 10 keV).

2.1 The sample

Since the goal of this paper is the study of the possible dependence of Γ , K_{bol} , α_{OX} and the disk/corona luminosity ratio on the accretion rate, we restrict the analysis to the sub-sample of radio-quiet 154 type 1 AGNs for which all these parameters have been already derived by fitting the UV-optical Spectral Energy Distribution (SEDs) of the sources (Marchese et al. 2012) and by studying the X-ray and optical spectra. The radio-loud AGNs of the sample (see Galbiati et al. 2005) were not considered to avoid possible contamination from the relativistic jet to the SED. The analysis of the SEDs was carried out on a subset of objects for which optical and UV data are available (either a detection or an upper limit) from existing catalogues (Sloan Digital Sky Survey, SDSS and Galaxy Evolution Explorer, GALEX). Since the availability of these data depends mainly on the position of the source in the sky and not on its intrinsic properties, this subset can be confidently considered as a representative sub-sample of the original one (see Marchese et al. 2012). In addition, in order to minimize the uncertainties on the values of L_{bol} , we have further restricted the analysis on a sub-sample of objects for which the possible effects of absorption are negligible, i. e. type 1 AGNs with an intrinsic absorbing column density, measured from the X-ray spectra, below $5 \times 10^{20} \text{ cm}^{-2}$. Finally, we have excluded from the analysis the small fraction ($\sim 8\%$) of “elusive” type 1 AGNs, i.e. those sources whose optical spectrum is dominated by the host galaxy (see Severgnini et al. 2003, Caccianiga et al. 2007), due to the impossibility of computing the BH mass through the Single Epoch spectral method (SE, e.g. see Peterson 2010 and Marziani & Sulentic 2012). In total, the final sample contains 71 objects. A Kolmogorov-Smirnov test indicates that this subsample is not statistically different (at 95% confidence level) from the original one from what concerns the Eddington ratio (Fig. 1) and the redshift (Fig. 2) distributions. We have also evaluated the possible impact of the exclusion of “elusive” AGNs from the analysis (see Section 3). The final sample used in this work consists of type 1 AGNs with rest-frame 2–10 keV luminosities ranging from $6 \times 10^{41} \text{ erg s}^{-1}$ to $9 \times 10^{46} \text{ erg s}^{-1}$ and redshift from 0.04 and 2.

2.2 Parameters

In this section, we describe the methods adopted to determine the parameters of interest (all reported in Table C1).

- L_{bol} and \dot{M} : bolometric luminosities were obtained as the sum of the accretion disk luminosity (L_{disk}) and the 0.1 – 100 keV X-ray luminosity. L_{disk} was obtained by fitting the optical-UV data with a disk model (Marchese et al. 2012), while L_{X} was obtained by extrapolating the results obtained in the 2–10 keV energy range analyzing the XMM-Newton data (Corral et al. 2011). As described in Marchese et al. (2012), the uncertainties on the bolometric luminosities take into account both the statistical errors on photometry and additional sources of error due to the correction for the intrinsic extinction and the long term variability (since the used photometric data are not simultaneous).

From bolometric luminosities we estimate the absolute accretion rate, defined as

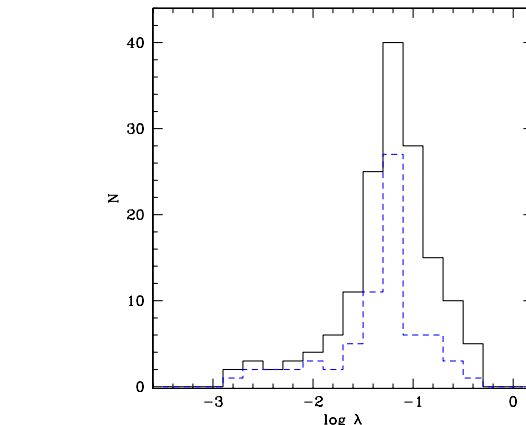


Figure 1. Eddington ratio distribution for the total sample presented in Marchese et al. (2012) (solid black line, 154 AGNs) and for the sub-sample used here (dashed blue line, 71 AGNs). The K-S test gives a probability for the null hypothesis (i.e. the two distributions are drawn from the same parent population) of 0.12.

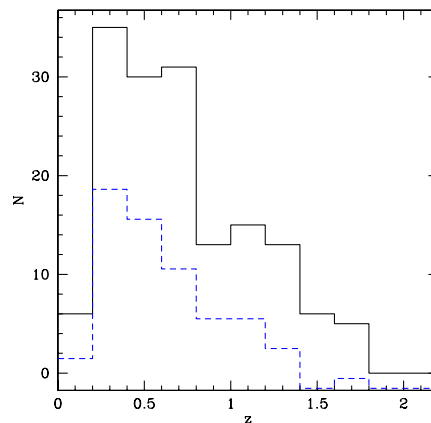


Figure 2. Redshift distribution for the total sample presented in Marchese et al. (2012) (solid black line, 154 AGNs) and for the sub-sample used here (dashed blue line, 71 AGNs). The K-S test gives a probability for the null hypothesis (i.e. the two distributions are drawn from the same parent population) of 0.35.

$$\dot{M} = \frac{L_{\text{bol}}}{\eta c^2} \quad (1)$$

where η is the efficiency of the mass to energy conversion, assumed to be 0.1. The uncertainties associated to the values of \dot{M} in Table C1 are those related to the bolometric luminosity i.e. we do not assume any error on η . The uncertainty on this value is difficult to assess. Marconi et al. (2004) estimate a range of values for η between 0.04 and 0.16 and, therefore, an additional uncertainty on \dot{M} up to a factor ~ 2 could be expected, besides that reported in Table C1. We note that, as explained above, the bolometric luminosities include the X-ray emission. Therefore, by using these bolometric luminosities to compute \dot{M} we are implicitly assuming that the energy budget carried by the X-ray emission is directly related to the accretion process.

- M_{BH} and Eddington ratio λ : black hole masses of the XBS type 1 AGNs are computed in Caccianiga et al. (2013)

using the Single Epoch (SE) method (Peterson 2010 and Marziani & Sulentic 2012). This method assumes that the Broad Line Region (BLR) is gravitationally influenced by the SMBH, so the virial theorem can be applied. The velocity dispersion is derived from the broad emission line widths while the BLR size is estimated from the continuum luminosity. The choice of emission lines used for M_{BH} estimate depends on the redshift of the source. In this sample we used $\text{H}\beta$ (for $0 < z \leq 0.8$) and MgII at 2798\AA lines (for $0.8 < z \leq 2$). In particular, we adopted the relation discussed in Vestergaard & Peterson (2006) for the $\text{H}\beta$:

$$\text{Log}M_{\text{BH}} = 6.91 + 2\text{Log}\frac{\text{FWHM}(\text{H}\beta)}{1000\text{km/s}} + 0.50\text{Log}\frac{\lambda L_{5100\text{\AA}}}{10^{44}\text{erg/s}} \quad (2)$$

and the relation presented in Shen et al. (2011) for the $\text{MgII}\lambda 2798\text{\AA}$ line:

$$\text{Log}M_{\text{BH}} = 6.74 + 2\text{Log}\frac{\text{FWHM}(\text{MgII})}{1000\text{km/s}} + 0.62\text{Log}\frac{\lambda L_{3000\text{\AA}}}{10^{44}\text{erg/s}} \quad (3)$$

the latter equation has been obtained by Shen et al. (2011) in such a way that the zero-order point (the virial factor) is the same as in the $\text{H}\beta$ relation presented above so that the masses are consistently derived from these two equations (see the discussion in Shen et al. 2011). In both relations, the line widths refer to the broad component, and it is assumed that a narrow component has been subtracted during the fitting procedure and that the iron emission has been taken into account. All the details on how the FWHM of the emission lines have been computed are given in Caccianiga et al. (2013). The monochromatic luminosities at 5100\AA ($L_{5100\text{\AA}}$) and 3000\AA ($L_{3000\text{\AA}}$) respectively are derived from the SED-fitting presented in Marchese et al. (2012).

The SE method is intrinsically affected by a large uncertainty, usually estimated between 0.35 and 0.46 dex (Park et al. 2012), essentially due to the unknown geometry of the BLR. Since the presence of large uncertainties can reduce significantly the strength of the correlations involving black hole masses (and the derived quantities) we have estimated the impact of these errors on the analysis presented here (see Section 3.2).

From the black hole masses we can estimate the accretion rate normalized to Eddington luminosity, defined as

$$\lambda = \frac{L_{\text{bol}}}{L_{\text{Edd}}}, \quad (4)$$

where L_{Edd} is the Eddington luminosity:

$$L_{\text{Edd}} = \frac{4\pi G c M_{\text{BH}} m_{\text{p}}}{\sigma_e} = 1.26 \cdot 10^{38} \left(\frac{M_{\text{BH}}}{M_{\odot}} \right) \text{erg} \cdot \text{s}^{-1}. \quad (5)$$

• Γ , $L_{(2-10)\text{keV}}$, K_{bol} , α_{OX} and disk/corona luminosity ratio: the values of $\Gamma_{(0.5-10)\text{keV}}$ and $L_{(2-10)\text{keV}}$ are taken from the spectral X-ray analysis presented in Corral et al. (2011). The bolometric corrections and the values of α_{OX} are available from Marchese et al. (2012). In particular, the bolometric correction is defined as:

$$K_{\text{bol}} = \frac{L_{\text{bol}}}{L_{(2-10)\text{keV}}} \quad (6)$$

while α_{OX} is defined as:

$$\alpha_{\text{OX}} = \frac{\text{Log}(f_o/f_x)}{\text{Log}(\nu_o/\nu_x)} \quad (7)$$

where f_o and f_x are, respectively, the rest frame monochromatic fluxes at $\nu_o = 1.20 \times 10^{15}$ Hz (corresponding to $\lambda_o = 2500\text{\AA}$) and $\nu_x = 4.84 \times 10^{17}$ Hz (corresponding to $E = 2$ keV).

Finally, the disk/corona luminosity ratios, defined as the ratio between the accretion disk luminosity, L_{disk} , and the 0.1-100 keV X-ray luminosity (L_X), are computed on the basis of the luminosities presented, again, in the Marchese et al. (2012) work.

3 STATISTICAL ANALYSIS

We perform a non parametric Spearman rank test on each correlation between X-ray properties (spectral index Γ , K_{bol} , α_{OX} , disk/corona luminosity ratio) and accretion rate (absolute \dot{M} and normalized to Eddington luminosity, λ). When the correlation is statistically significant, we perform a fit to the data (using both the ordinary least-squares, OLS, and the bisector methods, Isobe et al. 1990) to derive the functional dependence. We define a *very significant correlation* if the probability of null hypothesis (the two quantities are not correlated) is $P \leq 0.10\%$, a *significant correlation* if $P \leq 1.00\%$ and a *marginal correlation* if $P \leq 5.00\%$. For convenience, the main correlation coefficients and probabilities computed in this paper are summarized in Tab. 1. During the analysis, we evaluate the impact of some possible biases that we detail in the following subsections.

3.1 Flux limited nature of the sample

The XBS is a flux limited sample. The strong $L - z$ correlation, induced by the presence of a flux limit, may create spurious correlations or cancel real ones. This is not a problem for the correlations involving the X-ray loudness (K_{bol} , α_{OX} and disk/corona luminosity ratio) since we find that these parameters are not dependent on z (See Table 1). On the contrary, the values of Γ turned out to be marginally dependent on z (see Section 4.1) and, therefore, the correlations involving this quantity are potentially affected by the aforementioned problem. To exclude this possible effect, we use the partial correlation analysis (Kendall & Stuart 1979, see also Appendix B) which allows to evaluate the correlation between two parameters excluding a third variable on which both parameters depend (in this case, the redshift). As further check of the effect of z on the correlations, we analyse the correlations involving Γ in a relatively narrow bin of z ($0 \leq z < 0.4$).

3.2 Error impact on correlation coefficient

As explained above, some parameters, like the black hole mass and λ are characterized by uncertainties comparable with their variance. This clearly reduces the strength of a correlation by decreasing the values of the correlation parameters. Under the hypothesis of independent errors, and if the average error on the quantities is known, it is possible to have an estimate of the intrinsic correlation parameter using the following relation:

$$r_i = r_{\text{obs}} \sqrt{\left(1 + \frac{\epsilon_x^2}{\sigma_x^2}\right) \left(1 + \frac{\epsilon_y^2}{\sigma_y^2}\right)} \quad (8)$$

where ϵ_x , ϵ_y are the average errors on the two variables, σ_x^2 and σ_y^2 are the intrinsic variances on the two variables, r_{obs} is the observed coefficient and the term under square root is the correction factor. The intrinsic variances can be obtained from the observed variances, $\sigma_{x,o}^2$ and $\sigma_{y,o}^2$, by subtracting quadratically the errors, i.e.: $\sigma_x^2 = \sigma_{x,o}^2 - \epsilon_x^2$ and $\sigma_y^2 = \sigma_{y,o}^2 - \epsilon_y^2$.

The relation (8) can be derived from linear correlation coefficient, assuming independent errors on variables. Using Montecarlo simulations we have verified that it can be also applied to Spearman coefficients in case of a non-linear relation (Appendix A).

The correction presented above is particularly important for the correlations involving the Eddington ratio, since its computation is based on the highly uncertain black-hole mass estimate. In this work we assume an intrinsic uncertainty on the black-hole mass of 0.40 dex which corresponds to a correction factor for the Eddington ratio of about ~ 1.57 .

We note that the correction discussed above can be used only to have an estimate of the intrinsic strength of the correlation under study. The probability associated to the correlation coefficient (to assess the actual presence of a correlation), instead, is still the one associated to the value of r_{obs} . Therefore, we will apply this correction only to the correlations that have been established to be statistically significant on the basis of the probabilities associated to the values of r_{obs} .

3.3 Induced correlations

\dot{M} and λ are inter-related quantities since they both depend on bolometric luminosity. A possible correlation, e.g. between Γ and λ , can create an unreal correlation between Γ and \dot{M} . To verify this situation, we use partial correlation analysis which allows to calculate the correlation degree between the parameters of X-ray emission and λ , excluding the dependence on \dot{M} and *vice-versa*. If the correlation disappears by excluding the dependence on the other variable, it is possible that the observed correlation is just induced by the other variable. Conversely, if the correlation remains, then both the observed correlations are likely to be real and not induced by the other variable.

3.4 Elusive AGNs

As already mentioned, we have excluded from the analysis a number of type 1 AGNs whose optical spectrum is dominated by the light from the host galaxy. As discussed in Severgnini et al. (2003) and Caccianiga et al. (2007) these sources appear in the optical band as “normal” (i.e. non active galaxies) because the nuclear light is diluted by the light coming from the host-galaxy. The spectrum shows no emission lines (the so-called XBONG sources) or few emission lines that do not allow the clear recognition of the AGN and to derive the correct spectral classification. In Caccianiga et al. (2007) we have used the X-ray spectral analysis to assess the actual presence of the AGN and to characterize it as “type 2” (absorbed, $N_H > 4 \times 10^{21} \text{ cm}^{-2}$) or “type 1” (un-absorbed, $N_H < 4 \times 10^{21} \text{ cm}^{-2}$) AGN. As expected, the frequency of “elusive” AGNs is higher in type

2 AGNs, since the absorption makes the dilution more effective to hide the AGN. However, also a fraction ($\sim 8\%$, see Caccianiga et al 2007) of type 1 AGNs is affected by this problem and this fraction increases rapidly when we consider type 1 AGNs of lower and lower X-ray luminosity, becoming very high ($> 50\%$) for $L_{(2-10)\text{keV}}$ lower than $10^{43} \text{ erg s}^{-1}$. In the sample considered here, i.e. the XBS type 1 AGNs from Marchese et al. (2012) with low values of N_H , there are 7 elusive AGNs that we have excluded from the analysis. Even if few, these objects could in principle change the results of the statistical analysis if they are not randomly distributed. We know, for instance, that these objects typically have the lowest values of the optical-to-X-ray flux ratio i.e. the lowest values of K_{bol} and the “flattest” values of α_{OX} (all but one have $\log K_{\text{bol}} < 1.3$ and $\alpha_{OX} > -1.4$). In order to evaluate the impact of the exclusion of these objects from the analysis, we have derived a rough estimate of the black-hole mass using the absolute magnitude in the K-band and adopted the relation discussed in Graham (2007):

$$\log M_{BH} = -0.37(K + 24) + 8.29 \quad (9)$$

where M_{BH} is given in units of solar masses and K is the absolute K-band magnitude. We have then estimated the values of Eddington ratio and \dot{M} . As expected, these objects have low accretion rates with respect to the rest of the sample ($\log \lambda < -1.7$ and $\log \dot{M} < -1.3$). We found that the elusive AGNs in general follow the trends observed in the total sample, so their impact on the analysis is not important. However, during the analysis presented in the following sections we will discuss, case by case, the effect of introducing the elusive AGNs on the correlation parameters.

4 RESULTS

4.1 Spectral index Γ

The spectral index Γ is found to marginally correlate with the Eddington ratio ($r_{\text{obs}} = 0.27$, $P = 1.64\%$, Fig. 3) while the correlation between Γ and \dot{M} is not significant ($r_{\text{obs}} = 0.17$, $P = 15.86\%$). Since Γ marginally depends also on z ($r_{\text{obs}} = -0.27$, $P = 1.64\%$) it is important to verify whether the observed Γ - λ correlation is in some way influenced by the luminosity- z correlation induced by the flux-limited nature of the sample (see discussion in Section 3.1). In Fig. 4 we present the Γ - λ correlation for sources between $0 \leq z < 0.4$. This is the range that contains the greatest number of object and offers the widest coverage of Γ - λ plane at the same time. The correlation in this bin of z is highly significant ($r_{\text{obs}} = 0.71$, $P < 0.10\%$).

To further check this correlation, we have used the partial correlation method to exclude the dependence on z from the analysis on the total sample of 71 AGNs. Again, we find a significant correlation with $r_{\text{obs}} = 0.36$ ($P = 0.10\%$). We conclude that the Γ - λ correlation is not induced by z . Rather, the effect of z is to weaken the correlation (see Fig. 3).

It is interesting to establish the origin of the Γ - z dependence. The spectral index Γ was computed using data in the range between 0.5 and 10 keV at rest-frame. In this energy range the X-ray spectrum could be contaminated by the presence of the soft-excess component. The origin of

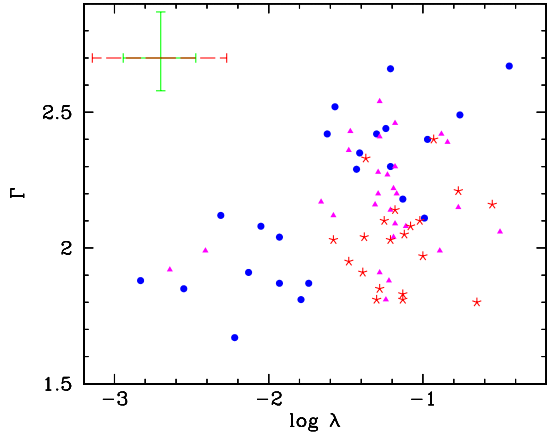


Figure 3. Plot of Γ against λ . A typical error is shown in the upper left corner: the green solid error bar is the statistical error, the red dashed one corresponds to the total error on λ (which includes the uncertainty related to the virial method used to estimate the black hole masses). The filled points (blue in the colour version) are sources with $0 \leq z < 0.4$, triangles (magenta in the colour version) are sources with $0.4 \leq z < 0.8$ and the stars (red in the colour version) are sources with $0.8 \leq z < 2$.

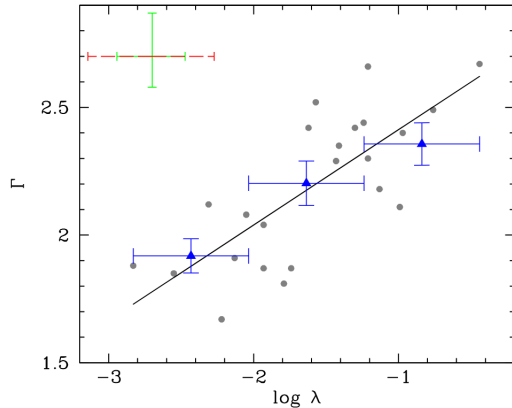


Figure 4. Plot of Γ against λ in the range $0 \leq z < 0.4$. A typical error is shown in the upper left corner: the green solid error bar is the statistical error, the red dashed one corresponds to the total error on λ (which includes the uncertainty related to the virial method used to estimate the black hole masses). The solid line represents the OLS best fit relation. Blue triangles are the binned data.

this component is still unclear. The classical interpretation of the soft excess is represented by the high-energy tail of black body emission of the disk accretion (Czerny & Elvis 1987, Grupe et al. 2010). However, this interpretation was questioned when several studies showed that the observed temperature of resulting black body is remarkably constant across orders of magnitude of luminosities and BH masses (Gierliński et al. 2004, Crummy et al. 2006). In the spectral analysis discussed in Corral et al. (2011) the soft excess component has been included in the model only if statistically required by the fit. This means that, if the number of counts is not large enough, the presence of the soft excess could be undetected and, thus, not included as additional

component in the fitting procedure. In these cases the fit is expected to produce a steeper value of Γ . Notably, the influence of this component depends on z : with increasing z , the soft excess is confined to lower energies and it becomes negligible for $z > 1 - 2$ (Mateos et al. 2010, Scott et al. 2011). Therefore, the presence of the soft excess can produce a spurious anti-correlation between Γ and z making steeper values of Γ at low redshifts. In order to test whether the soft excess is at the origin of the observed Γ - z dependence, we have re-computed the values of Γ by restricting the data to energies above 2 keV (rest-frame) in order to exclude the possible contamination due to the soft excess. The resulting values of $\Gamma_{(2-10)\text{keV}}$ are poorly determined due to the low statistics in the hard part of the spectrum. Nevertheless, they can be used as an independent test of our conclusions. We find that the values of $\Gamma_{(2-10)\text{keV}}$ do not depend on z ($r_{\text{obs}} = -0.13$, $P = 28.92\%$), while they depend on λ , although with a lower significance ($r_{\text{obs}} = 0.24$, $P = 4.14\%$) when compared to Γ . In principle, given the larger errors on $\Gamma_{(2-10)\text{keV}}$ if compared to Γ , we do expect any correlation to be weaker when considering this parameter. Using equation (8) discussed in Section 3.2, it is possible to have an estimate of the impact of the larger errors on the correlations. Since the average error on $\Gamma_{(2-10)\text{keV}}$ ($\epsilon \sim 0.20$) is a factor ~ 2.5 larger than the average error on Γ ($\epsilon \sim 0.08$) we expect a decrease by a factor ~ 1.3 of the correlation coefficient just due to the increased errors. Thus, if $\Gamma_{(2-10)\text{keV}}$ had the same dependence on z and λ as Γ ($r_{\text{obs}} = -0.27$ and $r_{\text{obs}} = 0.36$, respectively) we should expect to observe correlation coefficients reduced by a factor 1.3 i.e. $r_{\text{obs}} = -0.21$ and $r_{\text{obs}} = 0.28$ respectively. While the observed coefficient for the $\Gamma_{(2-10)\text{keV}}-\lambda$ correlation (0.24) is quite close to the expected one (0.28), the $\Gamma_{(2-10)\text{keV}}-z$ correlation coefficient (-0.13) is nearly half than the expected one (-0.21). We consider this as an indication that the $\Gamma_{(0.5-10\text{keV})}-\lambda$ and $\Gamma-\lambda$ correlation has probably a similar strength while the dependence of the hard spectral index with redshift is much weaker (if any). These results support both the idea that the dependence between Γ and z is (mainly) induced by the presence of the soft excess and the idea that it is the spectral index of the primary X-ray component, and not the soft excess intensity, that correlates with the Eddington ratio. Clearly, better quality spectra, in particular at energies above 2 keV, are required to put these conclusions on a firmer ground.

Both Γ and, in particular, λ are characterized by uncertainties that are on average large with respect to the variance of the parameters. As explained in Section 3.2, the presence of such large errors reduces significantly the measured strength of the correlation, i.e. the value of r . In order to have a better estimate of the actual level of correlation between Γ and λ , we have thus applied the corrections described in Section 3.2 finding a *corrected* value of r_1 of 0.6. In case of linear correlation, the square of r_1 gives an indication of how much of the observed variance on Γ is regulated by the value of λ . We thus conclude that about 40% of the variance on the spectral index is explained by λ . This is the strongest correlation found in the sample. We have evaluated the impact of the elusive AGNs (Section 3.4) by adding these objects to the sample. We find that their addition improves the $\Gamma-\lambda$ correlation while the $\Gamma-\dot{M}$ correlation remains not significant. We conclude that the observed $\Gamma-\lambda$ correlation is not due to the exclusion of the elusive AGNs.

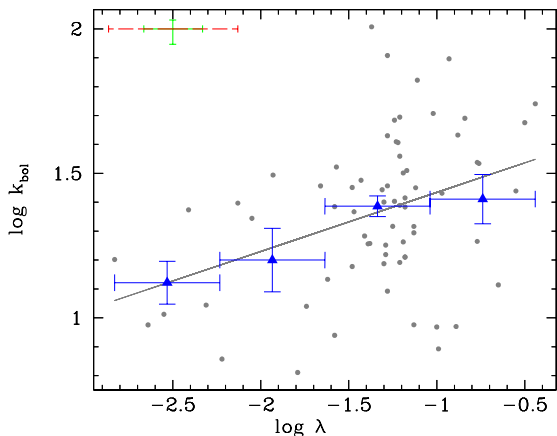


Figure 5. Plot of K_{bol} against λ . A typical error is shown in the upper left corner: the green solid error bar is the statistical error, the red dashed one corresponds to the total error on λ (which includes the uncertainty related to the virial method used to estimate the black hole masses). The solid line represents the OLS best fit relation. Blue triangles are the binned data.

We compute the ordinary least-squares (OLS) fit for the correlation $\Gamma - \lambda$ and we obtain

$$\Gamma = 0.25 \log \lambda + 2.48 \quad (10)$$

with an error of ± 0.05 on the slope, and the bisector from which

$$\Gamma = 0.75 \log \lambda + 3.15 \quad (11)$$

with an error of ± 0.04 on the slope.

4.2 Bolometric correction K_{bol}

We find a significant correlation between K_{bol} and λ ($r_{\text{obs}} = 0.33$, $P = 0.42\%$, Fig. 5), while the correlation between K_{bol} and \dot{M} is only marginally significant ($r_{\text{obs}} = 0.27$, $P = 2.14\%$).

By using the equation (8) to correct the correlation coefficient of $K_{\text{bol}} - \lambda$ correlation, we obtain $r_i = 0.52$ which suggests that $\sim 25\%$ of the variance on K_{bol} is explained by λ . We compute the ordinary least-squares (OLS) fit for the correlation $K_{\text{bol}} - \lambda$ and we obtain

$$\log K_{\text{bol}} = 0.18 \log \lambda + 1.61 \quad (12)$$

with an error of ± 0.06 on the slope, and the bisector from which

$$\log K_{\text{bol}} = 0.72 \log \lambda + 2.32 \quad (13)$$

with an error of ± 0.05 on the slope.

The slope obtained using the bisector method (0.72 ± 0.05) is in good agreement with that presented in Lusso et al. (2012) (0.75 ± 0.04) while the OLS slope is significantly ($\sim 2.5\sigma$) flatter (0.18 versus 0.39). The discrepancy is slightly reduced if we fit the data on the same range of K_{bol} observed in Lusso et al. (2012) (we find 0.24 ± 0.11). Again, we have verified that the observed correlations are not due to the exclusion of the elusive AGNs.

In conclusion, the results show that both the spectral index Γ and the bolometric correction K_{bol} depend significantly on λ : steep Γ (~ 2.5) and high K_{bol} ($\sim 30 - 60$) values

correspond to higher λ (~ 1), flat Γ (~ 1.7) and low K_{bol} values (~ 10) correspond to lower λ ($\sim 10^{-2}$). Since K_{bol} depends also on Γ it is possible that the $K_{\text{bol}} - \lambda$ correlation is induced by the (stronger) $\Gamma - \lambda$ correlation. Again, we have verified this hypothesis using the partial correlation analysis and found that the dependence between K_{bol} and λ can indeed be explained as induced to the $\Gamma - \lambda$ correlation.

In order to visualize these dependences we show in Fig. 6 two theoretical SEDs representing two extreme cases of low ($\lambda \sim 10^{-3}$, left panel) and high ($\lambda \sim 1$, right panel) accretion rate. We have built these SEDs using a Shakura-Sunyaev disk model with a maximum temperature of 3 eV (corresponding to the average temperature of the sample sources) and a power-law in the range between ~ 0.01 and 100 keV with a cut-off at 0.1 keV. The values of the spectral index of the X-ray power-law and the relative normalizations between the disk and the X-ray component are obtained from our $\Gamma - \lambda$ and $K_{\text{bol}} - \lambda$ fits, i.e. from (10) and (12). In this way the two SEDs of Fig. 6 can be considered as a visual representation of the correlation analysis discussed in the previous sections. To simplify the comparison between the two SEDs, we assumed the same disk emission in both cases. It is clear from the comparison of the two SEDs that the variation of K_{bol} with λ can be simply explained as due to a change of Γ , as suggested by the partial correlation analysis. We stress that the point where the disk emission intersects the corona emission is not fixed “a priori” but it comes from the values of Γ and K_{bol} obtained from the fits.

4.3 α_{OX}

Contrary to what is observed for the K_{bol} , we find a marginally significant anticorrelation between α_{OX} and λ ($r_{\text{obs}} = -0.25$, $P = 3.32\%$) while we find a significant anticorrelation between α_{OX} and \dot{M} ($r_{\text{obs}} = -0.41$, $P < 0.10\%$, Fig. 7). Even if we weight the correlation coefficients for the errors the dependence between $\alpha_{\text{OX}} - \dot{M}$ remains the strongest one ($r_i = -0.41$ versus -0.39). This result confirms what is usually found in the literature i.e. that the value of α_{OX} anti-correlates with the bolometric/UV luminosity while it has weaker dependence with the Eddington ratio. The inclusion of the elusive AGNs improves the significance of both $\alpha_{\text{OX}} - \lambda$ and $\alpha_{\text{OX}} - \dot{M}$ correlations.

Since both K_{bol} and α_{OX} are expected to be in some way proxies of the disk/corona relative intensity, the fact of finding two different dependences for these two quantities, one (K_{bol}) on the relative accretion rate and the other (α_{OX}) on the absolute accretion, seems difficult to reconcile. However, these two observational parameters are clearly related but not identical. The major difference is the fact that α_{OX} is defined at given monochromatic frequencies while K_{bol} is the ratio of two integrated quantities. For a fixed value of K_{bol} we can measure different values of α_{OX} depending on the actual spectral shape and *vice-versa*. In particular, the value of α_{OX} is less sensitive to the slope of the X-ray emission if compared to K_{bol} ($r_{\text{obs}} = -0.24$, $P = 4.04\%$ for $\alpha_{\text{OX}} - \Gamma$, and $r_{\text{obs}} = 0.53$, $P < 0.1\%$ for $K_{\text{bol}} - \Gamma$). As shown in the previous section, the dependence of K_{bol} to the Eddington ratio is probably induced by a change of Γ so it is probable that the weaker dependence of α_{OX} on λ is a consequence of the weaker dependence of α_{OX} on Γ .

On the other hand, the significant dependence of α_{OX}

	Γ	$\Gamma_{(2-10)\text{keV}}$	K_{bol}	α_{OX}	<i>Disk/corona</i>
	$r_{\text{obs}}^{(1)}, P$	r_{obs}, P	r_{obs}, P	r_{obs}, P	r_{obs}, P
	$r_i^{(2)}$	$r_i^{(2)}$	$r_i^{(2)}$	$r_i^{(2)}$	$r_i^{(2)}$
z	-0.27, 1.64%	-0.13, 28.92%	0.03, 80.26%	-0.22, 6.29%	0.18, 11.41%
λ	0.36, 0.10%	0.24, 4.14%	0.33, 0.42%	-0.25, 3.32%	0.28, 1.64%
	0.60	0.51	0.52	-0.39	0.44
\dot{M}	0.17, 15.86%		0.27, 2.14%	-0.41, < 0.10%	0.37, < 0.10%
	0.19		0.24	-0.41	0.37

Table 1. Spearman “rank” correlation coefficients and probabilities for the null hypothesis for the relations discussed in the text. ⁽¹⁾These values of r_{obs} are computed by excluding the dependence on redshift via partial correlation. ⁽²⁾These values of r are an estimate of the “intrinsic” correlation coefficients computed by taking into account the role of errors (see text for details).

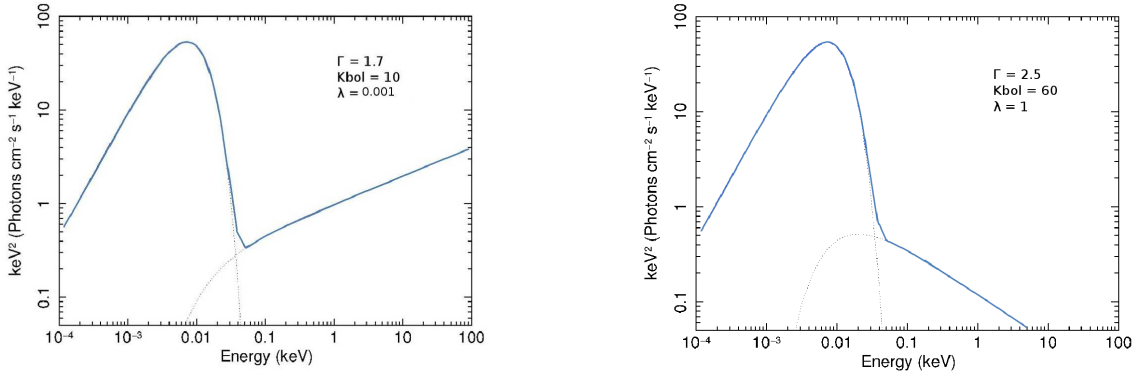


Figure 6. SEDs obtained using the results of the Γ - λ and $K_{\text{bol}} - \lambda$ best fits. The SED on the left represents the case of low accretion ($\lambda \sim 10^{-3}$): the K_{bol} value is low and Γ is flat. The SED on the right represents instead the case of high accretion rate ($\lambda \sim 1$): in this case K_{bol} is high and Γ is steep.

with \dot{M} suggests that the disk/corona relative intensity depends also on the absolute accretion rate. We test this hypothesis in the next section by studying directly the disk/corona luminosity ratio.

4.4 Disk-corona luminosity ratio

The dependences of K_{bol} and α_{OX} discussed in the previous sections seem to suggest a complex relationship between the disk/corona luminosity ratio and the accretion. From the one hand, there is a significant dependence on the Eddington ratio, probably related to a change of X-ray slope with λ . On the other hand, there could be also a dependence of the disk/corona luminosity ratio on the absolute level of accretion rate. We now want to study directly the dependence of the disk/corona luminosity ratio with accretion. As expected, the situation in this case is more complex than the K_{bol} and α_{OX} case. We find significant correlation with \dot{M} ($r_{\text{obs}} = 0.37$, $P < 0.10\%$, Fig. 8) and a marginally significant correlation with λ ($r_{\text{obs}} = 0.28$, $P = 1.64\%$, Fig. 9). We find a similar result if we add the elusive AGNs into the analysis. The strength of the two correlations, once corrected for the errors, is quite similar ($r_i \sim 0.4$) so it is difficult to establish if there is a dominant correlation that explains also the

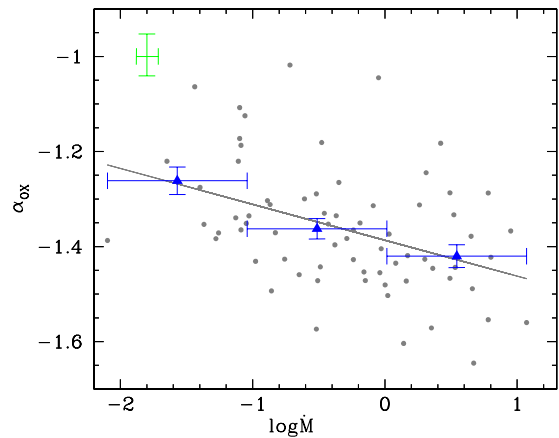


Figure 7. Plot of α_{OX} against \dot{M} . A typical error is shown in the upper left corner and it is the average statistical error on α_{OX} and \dot{M} . The solid line represents the OLS best fit relation. Blue triangles are the binned data.

other one. It is thus possible that both correlations are in fact present i.e. that the disk/corona relative intensity de-

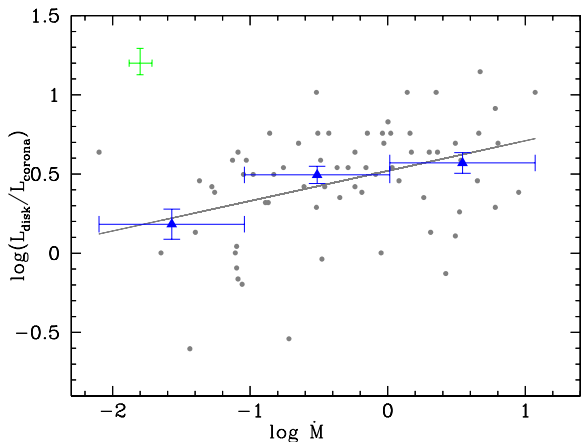


Figure 8. Plot of disk-corona luminosity ratio against \dot{M} . A typical error is shown in the upper left corner and it is the average statistical error on disk-corona luminosity ratio and \dot{M} . The solid line represents the OLS best fit relation. Blue triangles are the binned data.

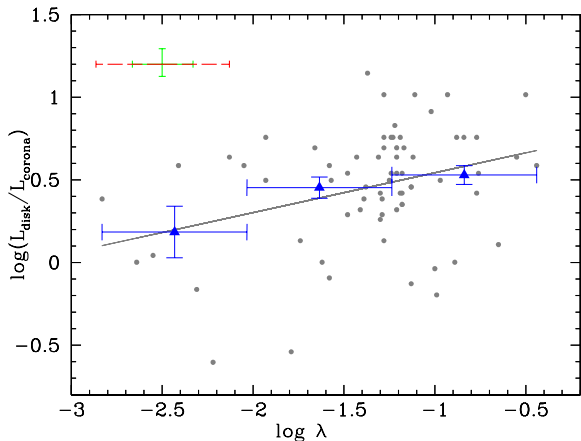


Figure 9. Plot of disk-corona ratio against λ . A typical error is shown in the upper left corner: the green solid error bar is the statistical error, the red dashed one corresponds to the total error on λ (which includes the uncertainty related to the virial method used to estimate the black hole masses). The solid line represents the OLS best fit relation. Blue triangles are the binned data.

pends both on λ and \dot{M} , as expected from the combination of the results obtained for K_{bol} and α_{OX} .

5 DISCUSSION AND CONCLUSIONS

In this paper we studied the link between X-ray emission and accretion rate in a statistically well-defined and complete sample of 71 type 1 AGNs extracted from the XMM-Newton Bright Serendipitous survey (XBS). The X-ray properties analyzed here are the spectral index Γ in the range 0.5 – 10 keV and 2 – 10 keV band and the X-ray “loudness” parametrized with both the bolometric correction K_{bol} (defined as the ratio between bolometric luminosity and 2 – 10 keV luminosity) and the two-points spectral index α_{OX} . We have also directly analysed the disk/corona luminosity ratio. The spectral index gives direct information

about the energy distribution of the electrons in the corona, while the other 3 parameters quantify, in different ways, the relative importance between disk and corona.

We have considered different possible biases which can influence final results, such as:

- soft excess contamination;
- redshift induced correlations (important in flux limited samples);
- impact of errors on correlation coefficients (especially on M_{BH} estimate);
- interconnected dependences due to the fact that the parameters considered in the analysis are not all independent;
- the impact of the exclusion of “elusive” AGNs from the analysis on the final results.

The results can be summarized as follows:

- the spectral index Γ depends significantly on accretion rate normalized to Eddington luminosity; in particular, $\sim 40\%$ of Γ variance could be explained by λ . This correlation is not due to the soft excess contamination, but it probably reflects a true dependence of the slope of the primary X-emission with λ . The Γ - λ dependence can be speculatively attributed to the effect of cooling of the electrons in the corona: for high values of λ , a large number of photons comes from the accretion disk and cools corona electrons rapidly, thus producing steep X-ray spectra while for low values of λ , less photons are available and this makes electron cooling inefficient, thus producing flat X-ray spectra (see for instance Cao 2009).
- the “X-ray loudness” depends both on λ and \dot{M} but the dependence with λ is probably just the consequence of the (stronger) Γ – λ dependence;
- The strength of the dependence between the “X-ray loudness” and λ or \dot{M} is different depending on whether we parametrize the X-ray loudness using the K_{bol} or the α_{OX} : while K_{bol} seems to depend mainly on λ , the values of α_{OX} show a stronger dependence with \dot{M} . The explanation is likely connected to the different sensitivity of these two parameters to the X-ray spectral index.

ACKNOWLEDGMENTS

We thank the referee for useful comments that improved the paper. We acknowledge Massimo Dotti, Francesco Haardt, Monica Colpi and Valentina Braito for useful discussions and Laura Maraschi and Tommaso Maccararo for the precious comments. The authors acknowledge financial support from ASI (grant n. I/088/06/0), from the Italian Ministry of Education, Universities and Research (PRIN2010-2011, grant n. 2010NHBSBE) and from the Spanish Ministry of Economy and Competitiveness through grant AYA2012-31447.

References

- Bianchi S., Bonilla N. F., Guainazzi M., Matt G., & Ponti G., 2009, *A&A*, 501, 915
 Brandt W. N., Mathur S., & Elvis M., 1997, *MNRAS*, 285, L25
 Caccianiga A., Severgnini P., Della Ceca R., Maccararo T., Carrera F. J., Page M. J., 2007, *A&A*, 470, 557

- Caccianiga A. et al., 2008, *A&A*, 477, 735
 Caccianiga A., Fanali R., Severgnini P., Della Ceca R., Marchese E., Mateos S., 2013, *A&A*, 549, A119
 Cao X. 2009, *MNRAS*, 394, 207
 Czerny B. & Elvis M., 1987, *ApJ*, 321, 305
 Corral A., Della Ceca R., Caccianiga A., Severgnini P., Brunner H., Carrera F.J., Page M.J., Schwobe A.D., 2011, *A&A*, 530, A42
 Crummy J., Fabian A. C., Gallo L., & Ross R. R. 2006, *MNRAS*, 365, 1067
 Della Ceca R. et al. 2004, *A&A*, 428, 383
 Galbiati E., et al., 2005, *A&A*, 430, 927
 Gierliński M. & Done C., 2004, *MNRAS*, 349, L7
 Graham A. W. 2007, *MNRAS*, 379, 711
 Grupe D., Leighly K. M., Burwitz V., Predehl P., Mathur S. 2004, *ApJ*, 128, 1524
 Grupe D., Komossa S., Leighly K. M., Page K. L., 2010, *ApJ*, 187, 64
 Gu M. & Cao X., 2009, *MNRAS*, 399, 349
 Haardt F. & Maraschi L., 1991, *ApJ*, 380, L51
 Hopkins P. F., Richards G. T. & Herquist L., 2007, *ApJ*, 654, 731
 Isobe T., Feigelson E. D. & Akritas M. G. & Babu G. J., 1990, *ApJ*, 364, 104
 Kelly B. C., Bechtold J., Trump J. R., Vestergaard, M. & Siemiginowska A., 2008, *ApJ*, 176, 355
 Kendall, M., Stuart, A., & *The Advanced Theory of Statistics*. MacMillan, New York.
 Laor A., Fiore F., Elvis M., Wilkes B. J. & McDowell J. C., 1997, *ApJ*, 477, 93
 Lusso E. et al., 2012, *MNRAS*, 425, 623
 Marchese E., Della Ceca R., Caccianiga A., Severgnini P., Corral A., Fanali R., 2012, *A&A*, 539, 48
 Marconi A., Risaliti G., Gilli R., Hunt L.K., Maiolino R., Salvati M., 2004, *MNRAS*, 351, 169
 Marziani P. & Sulentic J. W., 2012, *New A Rev.*, 56, 49
 Mateos S. et al., 2010, *A&A*, 510, A35
 Park S. et al., 2012, *ApJ*, 747, 30
 Peterson B. M., 2010, *IAU Symposium*, 267, 151
 Piconcelli E., Jimenez-Bailón E., Guainazzi M., Schartel N., Rodriguez-Pascual P.M., Santos-Lleo M., 2005, *A&A*, 432, 15
 Porquet D., Reeves J. N., O'Brien P. & Brinkmann, W. 2004, *A&A*, 422, 85
 Risaliti G., Yourng M. & Elvis M., 2009, *ApJ*, 700, L6
 Scott A. E, Steward G. C., Mateos S., Alexander D., Hutton S., Ward M.J., 2011, *MNRAS*, 417, 992
 Severgnini P., 2003, *A&A*, 406, 483
 Shen Y. et al., 2011, *ApJ*, 194, 45
 Shemmer O., Brandt W. N., Netzer H., Maiolino, R. & Kaspi S., 2008, *ApJ*, 682, 81
 Sulentic J. W., Marziani P. & Dultzin-Hacyan D., 2000, *A&AR*, 38, 521
 Vasudevan R. V. & Fabian A. C., 2007, *MNRAS*, 381, 1235
 Vaudevan R. V. & Fabian A. C., 2009, *MNRAS*, 392, 1124
 Vestergaard M. & Peterson B. M., 2006, *ApJ*, 641, 689
 Vignali C., Brandt W. N. & Schneider D. P., 2003, *ApJ*, 125, 433
 Wang, T., Brinkmann, W., & Bergeron, J. 1996, *A&A*, 309, 81
 Wang J. M., Watarai K. Y. & Mineshige S. 2004, *ApJ*, 607, L107
 Young M., Elvis M. & Risaliti G., 2010, *ApJ*, 708, 1388
 Zhou & Zhang, 2010, *ApJ*, 713, L11-L15

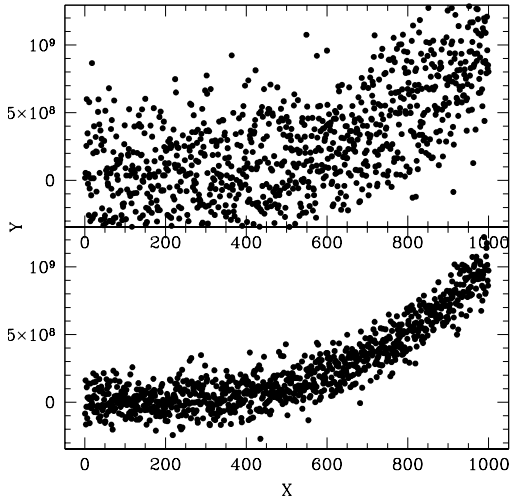


Figure A1. Numerical simulation (~ 1000 points) that shows the impact of a big error (comparable with the variance of the variable, in this example Y) on the Y-X correlation. In this example we assume a correlation coefficient $r \sim 0.87$ (lower panel) and we add an error on Y comparable with the intrinsic variance on Y. The resulting correlation (upper panel) is significantly reduced ($r \sim 0.62$).

APPENDIX A: ERROR IMPACT ON CORRELATION COEFFICIENT

Some parameters used in this analysis (like the black hole mass and the Eddington ratio) are characterized by very large errors, principally related to the method adopted to estimate the black hole masses. If the error is comparable to the variance of a variable, this can reduce the strength of a correlation by decreasing the values of the correlation coefficients. We estimate the intrinsic correlation parameter by using the relation:

$$r_i = r_{\text{obs}} \sqrt{\left(1 + \frac{\epsilon_x^2}{\sigma_x^2}\right) \left(1 + \frac{\epsilon_y^2}{\sigma_y^2}\right)}. \quad (\text{A1})$$

where ϵ_x , ϵ_y are the average errors on the two variables, σ_x^2 and σ_y^2 are the intrinsic (i.e. not folded with the errors) variances on the two variables, r_{obs} is the observed coefficient and the term under square root of this variable is the correction factor. This relation can be derived from linear correlation coefficient, assuming independent errors on variables. Using Montecarlo simulations we have verified that it can be also applied to Spearman coefficients in case of a non-linear relation. Fig. A1 represents a Montecarlo simulation where we show the case of a cubic correlation between two variables, X and Y, with an intrinsic correlation coefficient $r \sim 0.87$ (lower panel in Fig. A1). If we add an error on Y comparable to the variance on this variable, the coefficient correlation is reduced to $r \sim 0.62$ (upper panel in Fig. A1).

We repeated these simulations for different values of errors and the trend of the observed r_{obs} is shown in Fig. A2 (blue stars). In Fig. A2 we also report the values of r_i estimated according to equation (A1) (red points). The starting value of $r_i \sim 0.9$ is reasonably recovered.

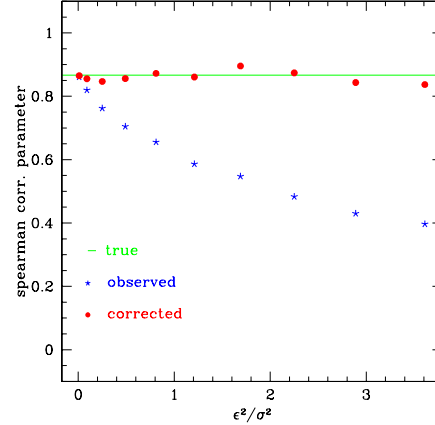


Figure A2. Results of numerical simulations that show the variation of the observed correlation coefficient (blue stars) with respect to the error²/variance ratio, assuming a starting value of $r \sim 0.87$. The red points represent corrected r values.

APPENDIX B: PARTIAL CORRELATIONS

As explained in Section 3.1, in a flux-limited sample like the XBS the luminosity is strongly correlated with redshift. This relation could give rise to spurious correlations. A way of dealing with the problem is to examine the correlations between luminosities excluding the dependence on redshift via partial correlation analysis. If r_{12} is the correlation coefficient between x_1 and x_2 and r_{13} and r_{23} are the correlation coefficients of the two variables with z , the correlation coefficient between x_1 and x_2 , excluding the effect of z is:

$$r_{12,3} = \frac{r_{12} - r_{13}r_{23}}{\sqrt{(1 - r_{13}^2)(1 - r_{23}^2)}}. \quad (\text{B1})$$

This equation can be generalized to more than three variables. For example, in the case of four variables it becomes:

$$r_{12,3,4} = \frac{r_{12,4} - r_{13,4}r_{23,4}}{\sqrt{(1 - r_{13,4}^2)(1 - r_{23,4}^2)}}. \quad (\text{B2})$$

APPENDIX C: THE SAMPLE

In this section we present the table including all the quantities used in the analysis discussed in the text.

Table C1. Main properties of the sample of 70 type 1 AGNs analysed in this work.

name	z	Γ	Γ_{2-10}	$\text{Log}K_{bol}$	$\text{Log}M_{BH}$	$\text{Log}\dot{M}$	$\text{Log}\lambda$	α_{OX}	$\text{Log}(L_{disk}/L_{corona})$
XBSJ000027.7-250442	0.336	1.87 ^{+0.06} _{-0.05}	1.57 ^{+0.27} _{-0.25}	1.32 ^{+0.09} _{-0.11}	8.63 ^{+0.10} _{-0.12}	-0.94 ^{+0.09} _{-0.12}	-1.93 ^{+0.13} _{-0.17}	-1.430	0.497
XBSJ000031.7-245502	0.284	2.29 ^{+0.08} _{-0.08}	1.86 ^{+0.42} _{-0.52}	1.48 ^{+0.10} _{-0.34}	8.02 ^{+1.32} _{-0.25}	-1.05 ^{+0.11} _{-0.33}	-1.43 ^{+1.32} _{-0.41}	-1.362	0.638
XBSJ000102.4-245850	0.433	2.12 ^{+0.07} _{-0.07}	1.89 ^{+0.28} _{-0.36}	0.94 ^{+0.06} _{-0.06}	8.16 ^{+0.15} _{-0.14}	-1.06 ^{+0.07} _{-0.06}	-1.58 ^{+0.17} _{-0.16}	-1.106	-0.093
XBSJ001831.6+162925	0.553	2.39 ^{+0.04} _{-0.04}	2.11 ^{+0.14} _{-0.17}	1.69 ^{+0.10} _{-0.08}	8.54 ^{+0.06} _{-0.05}	0.06 ^{+0.10} _{-0.09}	-0.84 ^{+0.12} _{-0.10}	-1.501	0.757
XBSJ002618.5+105019	0.473	2.04 ^{+0.04} _{-0.04}	1.95 ^{+0.16} _{-0.15}	1.50 ^{+0.10} _{-0.08}	9.03 ^{+0.10} _{-0.14}	0.20 ^{+0.10} _{-0.08}	-1.19 ^{+0.14} _{-0.16}	-1.469	0.757
XBSJ002637.4+165953	0.554	2.15 ^{+0.04} _{-0.03}	2.07 ^{+0.13} _{-0.13}	1.26 ^{+0.09} _{-0.11}	8.21 ^{+0.11} _{-0.41}	-0.20 ^{+0.08} _{-0.11}	-0.77 ^{+0.14} _{-0.42}	-1.363	0.420
XBSJ003418.9-115940	0.850	2.10 ^{+0.27} _{-0.16}	2.03 ^{+0.43} _{-0.51}	1.32 ^{+0.14} _{-0.16}	8.84 ^{+0.11} _{-0.13}	-0.05 ^{+0.14} _{-0.16}	-1.25 ^{+0.18} _{-0.21}	-1.310	0.497
XBSJ005009.9-515934	0.610	2.28 ^{+0.09} _{-0.08}	2.11 ^{+0.44} _{-0.42}	1.22 ^{+0.08} _{-0.06}	8.45 ^{+0.35} _{-0.08}	-0.48 ^{+0.08} _{-0.10}	-1.29 ^{+0.36} _{-0.58}	-1.287	0.289
XBSJ010432.8-583712	1.640	1.95 ^{+0.04} _{-0.04}	1.76 ^{n.d.}	1.18 ^{+0.10} _{-0.10}	9.94 ^{+0.09} _{-0.09}	0.82 ^{+0.09} _{-0.09}	-1.48 ^{+0.13} _{-0.13}	-1.285	0.289
XBSJ012025.2-105441	1.338	2.40 ^{+0.21} _{-0.18}	2.32 ^{+0.36} _{-0.31}	1.90 ^{+0.14} _{-0.14}	9.68 ^{+0.08} _{-0.08}	1.11 ^{+0.14} _{-0.14}	-0.93 ^{+0.16} _{-0.16}	-1.558	1.016
XBSJ012119.9-110418	0.204	2.66 ^{+0.23} _{-0.14}	3.56 ^{+1.54} _{-1.16}	1.69 ^{+0.12} _{-0.12}	8.13 ^{+0.08} _{-0.09}	-0.72 ^{+0.12} _{-0.12}	-1.21 ^{+0.14} _{-0.15}	-1.424	0.540
XBSJ013204.9-400050	0.445	2.42 ^{+0.17} _{-0.14}	2.48 ^{+0.52} _{-0.43}	1.63 ^{+0.13} _{-0.13}	8.05 ^{+0.13} _{-0.12}	-0.47 ^{+0.13} _{-0.13}	-0.88 ^{+0.18} _{-0.18}	-1.470	0.757
XBSJ020029.0+002846	0.174	2.42 ^{+0.10} _{-0.10}	2.22 ^{+0.66} _{-0.80}	1.13 ^{+0.06} _{-0.05}	7.65 ^{+0.17} _{-0.20}	-1.61 ^{+0.06} _{-0.05}	-1.62 ^{+0.18} _{-0.21}	-1.218	0.002
XBSJ021808.3-045845	0.712	1.91 ^{+0.04} _{-0.03}	n.d.	1.46 ^{+0.10} _{-0.08}	9.45 ^{+0.06} _{-0.05}	0.53 ^{+0.09} _{-0.08}	-1.28 ^{+0.11} _{-0.09}	-1.465	0.694
XBSJ021817.4-045113	1.080	1.83 ^{+0.04} _{-0.03}	1.78 ^{+0.08} _{-0.07}	0.98 ^{+0.06} _{-0.07}	9.23 ^{+0.06} _{-0.09}	0.46 ^{+0.07} _{-0.07}	-1.13 ^{+0.09} _{-0.11}	-1.181	-0.128
XBSJ021820.6-050427	0.646	1.81 ^{+0.04} _{-0.04}	1.70 ^{+0.14} _{-0.13}	1.40 ^{+0.06} _{-0.12}	8.76 ^{+0.06} _{-0.10}	-0.12 ^{+0.06} _{-0.12}	-1.24 ^{+0.08} _{-0.16}	-1.451	0.540
XBSJ021923.2-045148	0.632	2.41 ^{+0.07} _{-0.04}	2.20 ^{+0.23} _{-0.22}	1.63 ^{+0.10} _{-0.08}	8.81 ^{+0.07} _{-0.05}	-0.11 ^{+0.10} _{-0.08}	-1.28 ^{+0.12} _{-0.09}	-1.470	0.757
XBSJ024200.9+000020	1.112	2.03 ^{+0.05} _{-0.04}	1.91 ^{+0.13} _{-0.17}	1.38 ^{+0.07} _{-0.04}	9.79 ^{+0.06} _{-0.04}	0.57 ^{+0.07} _{-0.04}	-1.58 ^{+0.09} _{-0.06}	-1.439	0.587
XBSJ024207.3+000037	0.385	2.52 ^{+0.12} _{-0.08}	1.93 ^{+0.31} _{-0.27}	1.52 ^{+0.06} _{-0.07}	8.42 ^{+0.10} _{-0.10}	-0.79 ^{+0.06} _{-0.07}	-1.57 ^{+0.12} _{-0.12}	-1.368	0.497
XBSJ031015.5-765131	1.187	1.91 ^{+0.02} _{-0.02}	1.84 ^{+0.06} _{-0.06}	1.26 ^{+0.09} _{-0.12}	10.02 ^{+0.08} _{-0.12}	0.99 ^{+0.09} _{-0.09}	-1.39 ^{+0.12} _{-0.12}	-1.364	0.385
XBSJ033208.7-274735	0.544	1.99 ^{+0.09} _{-0.07}	1.92 ^{+0.19} _{-0.24}	1.37 ^{+0.07} _{-0.13}	9.60 ^{+0.07} _{-0.11}	-0.45 ^{+0.07} _{-0.13}	-2.41 ^{+0.10} _{-0.17}	-1.441	0.587
XBSJ050446.3-283821	0.840	1.97 ^{+0.11} _{-0.08}	1.87 ^{+0.46} _{-0.38}	0.97 ^{+0.08} _{-0.07}	8.20 ^{+0.35} _{-0.36}	-0.44 ^{+0.08} _{-0.06}	-1.00 ^{+0.36} _{-0.36}	-1.178	-0.037
XBSJ050501.8-284149	0.257	2.18 ^{+0.05} _{-0.05}	2.15 ^{+0.39} _{-0.35}	1.29 ^{+0.14} _{-0.11}	7.44 ^{+0.11} _{-0.09}	-1.33 ^{+0.14} _{-0.11}	-1.13 ^{+0.18} _{-0.14}	-1.350	0.457
XBSJ051955.5-455727	0.562	2.09 ^{+0.04} _{-0.04}	2.00 ^{+0.38} _{-0.33}	1.21 ^{+0.08} _{-0.10}	8.51 ^{+0.07} _{-0.08}	-0.31 ^{+0.08} _{-0.11}	-1.18 ^{+0.11} _{-0.14}	-1.262	0.351
XBSJ065400.0+742045	0.362	2.30 ^{+0.19} _{-0.12}	2.37 ^{+0.60} _{-0.49}	1.56 ^{+0.13} _{-0.13}	8.24 ^{+0.10} _{-0.10}	-0.61 ^{+0.12} _{-0.13}	-1.21 ^{+0.16} _{-0.16}	-1.456	0.694
XBSJ074352.0+744258	0.800	2.03 ^{+0.07} _{-0.07}	1.92 ^{+0.20} _{-0.25}	1.39 ^{+0.09} _{-0.12}	9.06 ^{+0.08} _{-0.09}	0.21 ^{+0.10} _{-0.12}	-1.21 ^{+0.13} _{-0.13}	-1.418	0.638
XBSJ080504.6+245156	0.980	2.08 ^{+0.10} _{-0.10}	1.77 ^{+0.32} _{-0.28}	0.96 ^{+0.04} _{-0.04}	8.39 ^{+0.14} _{-0.17}	-0.33 ^{+0.03} _{-0.05}	-1.08 ^{+0.14} _{-0.18}	-1.155	-0.075
XBSJ080608.1+244420	0.357	2.49 ^{+0.04} _{-0.03}	2.21 ^{+0.18} _{-0.23}	1.53 ^{+0.06} _{-0.07}	8.15 ^{+0.07} _{-0.07}	-0.25 ^{+0.06} _{-0.07}	-0.76 ^{+0.09} _{-0.10}	-1.380	0.540
XBSJ100100.4+252103	0.794	2.20 ^{+0.07} _{-0.04}	2.12 ^{+0.17} _{-0.16}	1.25 ^{+0.08} _{-0.07}	8.78 ^{+0.06} _{-0.05}	-0.15 ^{+0.08} _{-0.07}	-1.29 ^{+0.10} _{-0.09}	-1.346	0.385
XBSJ100309.4+554135	0.673	2.27 ^{+0.07} _{-0.06}	1.86 ^{+0.35} _{-0.42}	1.61 ^{+0.07} _{-0.08}	8.87 ^{+0.05} _{-0.05}	-0.01 ^{+0.08} _{-0.08}	-1.23 ^{+0.09} _{-0.09}	-1.454	0.757
XBSJ100828.8+535408	0.384	2.04 ^{+0.12} _{-0.09}	1.29 ^{+0.64} _{-0.54}	1.49 ^{+0.07} _{-0.08}	8.75 ^{+0.30} _{-0.24}	-0.82 ^{+0.07} _{-0.08}	-1.93 ^{+0.31} _{-0.25}	-1.491	0.757
XBSJ100921.7+534926	0.387	2.35 ^{+0.08} _{-0.05}	1.94 ^{+0.35} _{-0.34}	1.28 ^{+0.08} _{-0.10}	8.22 ^{+0.12} _{-0.12}	-0.83 ^{+0.08} _{-0.10}	-1.41 ^{+0.16} _{-0.16}	-1.309	0.320
XBSJ101838.0+411635	0.577	2.36 ^{+0.07} _{-0.06}	2.09 ^{+0.30} _{-0.26}	1.45 ^{+0.06} _{-0.07}	8.79 ^{+0.05} _{-0.06}	-0.33 ^{+0.07} _{-0.07}	-1.48 ^{+0.09} _{-0.09}	-1.332	0.540
XBSJ101850.5+411506	0.577	2.30 ^{+0.05} _{-0.03}	2.17 ^{+0.15} _{-0.20}	1.38 ^{+0.06} _{-0.07}	8.89 ^{+0.05} _{-0.04}	0.07 ^{+0.07} _{-0.08}	-1.18 ^{+0.09} _{-0.08}	-1.372	0.540
XBSJ101922.6+412049	0.239	2.12 ^{+0.16} _{-0.05}	n.d.	1.04 ^{+0.05} _{-0.04}	8.90 ^{+0.08} _{-0.75}	-1.05 ^{+0.05} _{-0.04}	-2.31 ^{+0.09} _{-0.75}	-1.186	-0.163
XBSJ103120.0+311404	1.190	1.85 ^{+0.12} _{-0.08}	1.76 ^{+0.20} _{-0.18}	1.09 ^{+0.09} _{-0.05}	9.27 ^{+0.09} _{-0.06}	0.35 ^{+0.09} _{-0.05}	-1.28 ^{+0.13} _{-0.08}	-1.240	0.132
XBSJ103154.1+310732	0.299	1.88 ^{+0.13} _{-0.12}	1.42 ^{+0.84} _{-0.76}	1.20 ^{+0.06} _{-0.07}	9.25 ^{+0.26} _{-0.19}	-1.22 ^{+0.06} _{-0.06}	-2.83 ^{+0.27} _{-0.20}	-1.369	0.385
XBSJ103932.7+205426	0.237	1.87 ^{+0.11} _{-0.09}	1.87 ^{+0.63} _{-0.54}	1.04 ^{+0.07} _{-0.05}	8.02 ^{+0.17} _{-0.13}	-1.36 ^{+0.07} _{-0.05}	-1.74 ^{+0.18} _{-0.14}	-1.273	0.132
XBSJ103935.8+533036	0.229	2.08 ^{+0.15} _{-0.10}	2.22 ^{+0.56} _{-0.43}	1.34 ^{+0.09} _{-0.12}	8.70 ^{+0.07} _{-0.09}	-0.99 ^{+0.09} _{-0.12}	-2.05 ^{+0.11} _{-0.15}	-1.333	0.587
XBSJ104026.9+204542	0.465	1.99 ^{+0.03} _{-0.03}	1.88 ^{+0.13} _{-0.13}	0.97 ^{+0.04} _{-0.05}	8.52 ^{+0.05} _{-0.08}	-0.01 ^{+0.04} _{-0.04}	-0.89 ^{+0.06} _{-0.09}	-1.043	0.002
XBSJ104509.3-012442	0.472	2.14 ^{+0.11} _{-0.06}	2.13 ^{+0.29} _{-0.31}	1.19 ^{+0.06} _{-0.06}	8.00 ^{+0.06} _{-0.05}	-0.85 ^{+0.05} _{-0.06}	-1.21 ^{+0.08} _{-0.08}	-1.301	0.320
XBSJ104912.8+330459	0.226	1.67 ^{+0.12} _{-0.09}	1.91 ^{+0.46} _{-0.39}	0.86 ^{+0.03} _{-0.03}	8.46 ^{+0.21} _{-0.18}	-1.40 ^{+0.02} _{-0.13}	-2.22 ^{+0.21} _{-0.18}	-1.060	-0.603
XBSJ105014.9+331013	1.012	2.33 ^{+0.37} _{-0.20}	2.45 ^{+0.95} _{-0.69}	2.01 ^{+0.10} _{-0.13}	9.72 ^{+0.13} _{-0.09}	0.71 ^{+0.10} _{-0.13}	-1.37 ^{+0.16} _{-0.16}	-1.643	1.146
XBSJ105239.7+572431	1.113	2.10 ^{+0.02} _{-0.02}	2.04 ^{+0.12} _{-0.16}	1.71 ^{+0.07} _{-0.09}	9.48 ^{+0.05} _{-0.06}	0.82 ^{+0.07} _{-0.09}	-1.02 ^{+0.09} _{-0.11}	-1.550	0.914
XBSJ105316.9+573551	1.204	1.80 ^{+0.02} _{-0.02}	1.97 ^{+0.14} _{-0.18}	1.11 ^{+0.05} _{-0.05}	8.82 ^{+0.12} _{-0.14}	0.53 ^{+0.05} _{-0.05}	-0.65 ^{+0.13} _{-0.15}	-1.285	0.109
XBSJ105624.2-033522	0.635	2.16 ^{+0.09} _{-0.06}	2.20 ^{+0.26} _{-0.23}	1.44 ^{+0.07} _{-0.08}	8.75 ^{+0.05} _{-0.05}	-0.20 ^{+0.07} _{-0.08}	-1.31 ^{+0.09} _{-0.09}	-1.425	0.638
XBSJ112022.3+125252	0.406	2.22 ^{+0.09} _{-0.08}	1.75 ^{+0.38} _{-0.50}	1.26 ^{+0.06} _{-0.07}	8.26 ^{+0.06} _{-0.06}	-0.57 ^{+0.06} _{-0.06}	-1.19 ^{+0.08} _{-0.08}	-1.295	0.420
XBSJ120359.1+443715	0.641	2.43 ^{+0.12} _{-0.12}	2.57 ^{+0.40} _{-0.34}	1.37 ^{+0.11} _{-0.10}	8.77 ^{+0.06} _{-0.06}	-0.34 ^{+0.11} _{-0.10}	-1.47 ^{+0.13} _{-0.12}	-1.396	1.600
XBSJ123116.5+641115	0.454	1.92 ^{+0.05} _{-0.05}	1.91 ^{+0.25} _{-0.22}	0.98 ^{+0.04} _{-0.04}	9.21 ^{+0.18} _{-0.13}	-1.07 ^{+0.05} _{-0.04}	-2.64 ^{+0.14} _{-0.14}	-1.217	0.002
XBSJ123759.6+621102	0.910	2.05 ^{+0.04} _{-0.04}	1.89 ^{+0.12} _{-0.15}	1.45 ^{+0.07} _{-0.08}	9.16 ^{+0.03} _{-0.05}	0.40 ^{+0.06} _{-0.08}	-1.12 ^{+0.08} _{-0.09}	-1.443	0.638

Table C1. continua

name	z	Γ	Γ_{2-10}	$\text{Log}K_{bol}$	$\text{Log}M_{BH}$	$\text{Log}\dot{M}$	$\text{Log}\lambda$	α_{OX}	$\text{Log}(L_{disk}/L_{corona})$
XBSJ123800.9+621338	0.440	$2.54^{+0.04}_{-0.05}$	$2.01^{+0.26}_{-0.33}$	$1.91^{+0.07}_{-0.09}$	$8.44^{+0.09}_{-0.10}$	$-0.48^{+0.07}_{-0.08}$	$-1.28^{+0.11}_{-0.13}$	-1.571	1.016
XBSJ124214.1-112512	0.820	$1.81^{+0.05}_{-0.05}$	$1.60^{+0.16}_{-0.15}$	$1.32^{+0.10}_{-0.08}$	$8.89^{+0.07}_{-0.06}$	$0.12^{+0.09}_{-0.08}$	$-1.13^{+0.11}_{-0.10}$	-1.431	0.457
XBSJ124607.6+022153	0.491	$2.46^{+0.12}_{-0.08}$	$1.81^{+0.57}_{-0.48}$	$1.42^{+0.06}_{-0.07}$	$8.40^{+0.10}_{-0.10}$	$-0.42^{+0.06}_{-0.07}$	$-1.18^{+0.12}_{-0.12}$	-1.326	0.420
XBSJ124641.8+022412	0.934	$2.21^{+0.07}_{-0.05}$	$2.00^{+0.19}_{-0.23}$	$1.54^{+0.04}_{-0.08}$	$9.11^{+0.02}_{-0.06}$	$0.70^{+0.03}_{-0.08}$	$-0.77^{+0.04}_{-0.10}$	-1.485	0.757
XBSJ124949.4-060722	1.053	$2.16^{+0.07}_{-0.06}$	$1.70^{+0.31}_{-0.28}$	$1.44^{+0.07}_{-0.08}$	$8.53^{+0.05}_{-0.06}$	$0.34^{+0.06}_{-0.08}$	$-0.55^{+0.08}_{-0.10}$	-1.422	0.638
XBSJ132101.6+340656	0.335	$2.44^{+0.04}_{-0.04}$	$2.18^{+0.57}_{-0.20}$	$1.68^{+0.07}_{-0.08}$	$8.49^{+0.07}_{-0.08}$	$-0.39^{+0.06}_{-0.09}$	$-1.24^{+0.09}_{-0.12}$	-1.351	0.757
XBSJ133807.5+242411	0.631	$2.08^{+0.10}_{-0.08}$	$1.84^{+0.32}_{-0.35}$	$1.82^{+0.07}_{-0.09}$	$8.93^{+0.04}_{-0.06}$	$0.18^{+0.07}_{-0.09}$	$-1.11^{+0.08}_{-0.11}$	-1.601	1.016
XBSJ134749.9+582111	0.646	$2.20^{+0.02}_{-0.02}$	$1.93^{+0.06}_{-0.06}$	$1.51^{+0.07}_{-0.08}$	$9.65^{+0.07}_{-0.07}$	$0.84^{+0.06}_{-0.08}$	$-1.17^{+0.09}_{-0.11}$	-1.419	0.694
XBSJ140102.0-111224 ¹	0.037	$1.91^{+0.02}_{-0.02}$	$1.74^{+0.12}_{-0.12}$	$1.40^{+0.19}_{-0.35}$	$7.71^{+0.96}_{-0.82}$	$-2.06^{+0.07}_{-0.09}$	$-2.13^{+0.96}_{-0.82}$	-1.382	0.638
XBSJ141531.5+113156	0.257	$1.85^{+0.02}_{-0.04}$	n.d.	$1.01^{+0.04}_{-0.05}$	$9.13^{+0.17}_{-0.15}$	$-1.06^{+0.05}_{-0.05}$	$-2.55^{+0.18}_{-0.16}$	-1.174	0.043
XBSJ144937.5+090826	1.260	$1.81^{+0.07}_{-0.04}$	$1.80^{+0.11}_{-0.10}$	$1.19^{+0.08}_{-0.06}$	$9.50^{+0.07}_{-0.06}$	$0.56^{+0.08}_{-0.06}$	$-1.30^{+0.11}_{-0.08}$	-1.332	0.261
XBSJ160706.6+075709	0.233	$2.42^{+0.09}_{-0.08}$	$2.02^{+0.62}_{-0.55}$	$1.40^{+0.06}_{-0.07}$	$7.70^{+0.10}_{-0.11}$	$-1.24^{+0.06}_{-0.07}$	$-1.30^{+0.12}_{-0.13}$	-1.382	0.420
XBSJ160731.5+081202	0.226	$2.67^{+0.22}_{-0.13}$	$2.32^{+0.72}_{-0.87}$	$1.74^{+0.09}_{-0.13}$	$6.99^{+0.09}_{-0.11}$	$-1.09^{+0.09}_{-0.08}$	$-0.44^{+0.13}_{-0.14}$	-1.335	0.587
XBSJ165406.6+142123	0.641	$1.88^{+0.12}_{-0.08}$	$1.93^{+0.39}_{-0.34}$	$1.61^{+0.13}_{-0.13}$	$8.90^{+0.09}_{-0.10}$	$0.04^{+0.13}_{-0.13}$	$-1.22^{+0.16}_{-0.16}$	-1.478	0.829
XBSJ165425.3+142159	0.178	$2.11^{+0.04}_{-0.02}$	$1.97^{+0.13}_{-0.13}$	$0.89^{+0.05}_{-0.04}$	$7.61^{+0.26}_{-0.36}$	$-1.02^{+0.04}_{-0.04}$	$-0.99^{+0.26}_{-0.36}$	-1.124	-0.196
XBSJ165448.5+141311	0.320	$1.81^{+0.07}_{-0.04}$	$1.78^{+0.20}_{-0.27}$	$0.81^{+0.02}_{-0.02}$	$8.75^{+0.05}_{-0.06}$	$-0.68^{+0.02}_{-0.02}$	$-1.79^{+0.05}_{-0.06}$	-1.016	-0.540
XBSJ205635.7-044717	0.217	$2.40^{+0.10}_{-0.08}$	$1.83^{+0.52}_{-0.73}$	$1.43^{+0.11}_{-0.11}$	$7.60^{+0.10}_{-0.09}$	$-1.01^{+0.11}_{-0.11}$	$-0.97^{+0.15}_{-0.14}$	-1.347	0.497
XBSJ213002.3-153414	0.562	$2.06^{+0.13}_{-0.12}$	$2.31^{+0.33}_{-0.30}$	$1.68^{+0.13}_{-0.14}$	$8.53^{+0.08}_{-0.07}$	$0.39^{+0.14}_{-0.13}$	$-0.50^{+0.16}_{-0.15}$	-1.567	1.016
XBSJ214041.4-234720	0.490	$2.17^{+0.05}_{-0.05}$	$1.91^{+0.19}_{-0.24}$	$1.46^{+0.10}_{-0.08}$	$9.31^{+0.06}_{-0.06}$	$0.01^{+0.10}_{-0.08}$	$-1.66^{+0.12}_{-0.10}$	-1.400	0.694
XBSJ225050.2-642900	1.251	$2.04^{+0.04}_{-0.04}$	$1.93^{+0.12}_{-0.12}$	$1.26^{+0.11}_{-0.11}$	$9.71^{+0.11}_{-0.08}$	$0.69^{+0.11}_{-0.10}$	$-1.38^{+0.16}_{-0.13}$	-1.374	0.457
XBSJ231342.5-423210	0.973	$2.14^{+0.08}_{-0.04}$	$2.00^{+0.16}_{-0.15}$	$1.21^{+0.08}_{-0.06}$	$9.12^{+0.11}_{-0.11}$	$0.30^{+0.08}_{-0.06}$	$-1.18^{+0.14}_{-0.13}$	-1.309	0.351

Table C1. Column 1: source name; Column 2: redshift; Column 3: X-ray spectral index between 0.5 and 10 keV; Column 4: X-ray spectral index between 2 and 10 keV; Column 5: Logarithm of the bolometric correction; Column 6: Logarithm of the black hole mass in units of solar masses; Columns 7: Logarithm of the absolute accretion rate in units of solar masses per year; Column 8: Logarithm of Eddington ratio; Column 9: two-point spectral index; Column 10: Logarithm of the disk/corona luminosity ratio. All errors are at 68% confidence level (please note that in Corral et al. 2011 the reported errors on Γ are at 90% confidence level). ¹The X-ray luminosity of XBSJ140102.0-111224 reported here is different from the value that appears in Corral et al. (2011) because of a typo discovered in that paper. Therefore, also the derived quantities, like K_{bol} , α_{OX} are different from what reported in Marchese et al. (2012).